



Prediction of Ballistic Limit of Composite GFRP Sandwich Panels under Hypervelocity Impact^{*}

LI Siyu¹, LI Xiaobin¹, ZHAO Pengduo², GAO Songlin¹

(1. Departments of Naval Architecture, Ocean and Structural Engineering,
Wuhan University of Technology, Wuhan 430063, China;
2. Navy Research Center, Beijing 100073, China)

Abstract: In the present study, analytical solutions were presented for the prediction of the penetration and perforation of composite glass fiber-reinforced plastic (GFRP) sandwich panels struck normally by flat-nosed cylindrical projectiles over a wide range of impacting velocities, projectile mass and core thickness. The analysis model involved a three-stage perforation process including perforation of the front steel skin, the GFRP core, and the back steel skin. The formulation were based on assumptions that the deformations of steel skins are localized and the projectile is considered as a rigid body in the perforation of GFRP composite laminate. The energy absorption of the front and back steel skins and the GFRP core were estimated with the upsetting effect of the projectile and the adiabatic shear effect of the steel skins taken into consideration. In addition, based on the energy balance, the ballistic limit of the sandwich panel were obtained and compared with the available experimental results. The results show that the analytical predictions are in good agreement with the available experimental data.

Keywords: ballistic impact; sandwich panel; glass fiber reinforced; ballistic limit

CLC number: O385; TB33

Document code: A

Sandwich composite structures are increasingly used in marine, military and aerospace fields due to their lightweight, high strength and energy absorption capability^[1-5]. A sandwich structure usually consists of two thin and stiff skins (the front skin and the back skin) and a thick and light core. The main function of the skins in a sandwich composite is to carry the bending moment while the core undertakes the duty of fixing the separated skins, carrying the transverse shear load, and performing otherstructural or functional duties such as impact tolerance, radiation shielding, etc^[6]. Because of military demand, the sandwich structures are frequently subjected to impact loadings such as fragments from blast debris, shrapnel and bullets. In these cases, the sandwich panel with steel skins and a fabric-reinforced plastic (FRP) composite core is an obvious choice.

A variety of FRP sandwich composites have been used for armor construction due to their highly complex processes, but the prediction of the residual velocity after penetration remains to be a tough problem because of its complicate process. A number of studies on the ballistic limit of sandwich structures are based on experimental tests^[7-8]. The experimental method requires a broad test program, which is time-consuming and costly. Numerical simulations may be useful in solving this problem but,

* Received date: 2017-01-12; Revised date: 2017-03-27

Foundation item: National Natural Science Foundation of China(11302259)

Biography: LI Siyu(1991—), male, master, major in structural safety and reliability. E-mail: lisiyufly@163.com

Corresponding author: LI Xiaobin(1971—), male, doctor, professor, major in structural safety and reliability.

E-mail: lxbmark@163.com

unfortunately, they still require considerable resources in terms of computing time (CPU) and manpower. To reduce the cost and time, it is essential to use the analytical method.

Researchers have done many experimental and analytical studies on the ballistic impact behavior of composites^[9-17]. Wen^[9-10] presented simple relationships for predicting the penetration and perforation of monolithic FRP laminates struck normally by projectiles with different nose shapes over a wide range of impact velocities. Gu^[11] presented an analytical model to calculate the decrease of the kinetic energy and residual velocity of a projectile penetrating the targets composed of multi-layered planar woven fabrics. Naik *et al.*^[12-13] studied the energy absorbed by different mechanisms, ballistic limit velocity and contact duration of typical woven fabric E-glass/epoxy thick composites using an analytical method. Gama and Gillespie^[14] found that the ballistic damage mechanisms can be mimicked by conducting a series of quasi-static punch shear experiments at different support spans. In their study, a quasi-static punch shear test (QS-PST) methodology was developed to quantify and partition the penetration energy into elastic and absorbed energies as a function of penetration displacement and support span. Besides, some researchers used the numerical simulation method to determine the ballistic limit of composite materials^[15-17], and the simulation results usually show good agreement with the test data.

Lots of work has been done on the problem of the ballistic limit of composite sandwich panels by many researchers^[7, 18-24]. Goldsmith *et al.*^[18] investigated the ballistic limit of cellular sandwich plates with honeycomb or flexible sheets of aluminum cores using the experiment. They found that the ballistic limit of the sandwich plates was not significantly affected by the type, cell size or wall diameter of the composite, as the principal mechanism resisting the perforation of the composite was piercing the facing plates.

Zhou and Stronge^[20] studied the effect of the impact angle and nose shape on the ballistic limit by experimental and numerical methods. The results suggested that during the perforation by a flat-nosed projectile, layered plates caused more energy loss than monolithic plates of the same material and total thickness. There was no significant difference in the measured ballistic limit speed between the monolithic plates and the layered plates at the oblique impact by a hemispherical-nosed projectile.

Skvortsov *et al.*^[19] developed an analytic model to deal with the partition of the energy of absorption, allowing for quantitative estimation of the energy fraction consumed via elastic response of the panel and the one consumed via irreversible damage. Numerical results are corroborated with experimental data obtained from intermediate-velocity impact tests performed for sandwich panels with FRP composite laminate faces and foam cores.

Buitrago *et al.*^[22] analyzed the perforation of composite sandwich structures subjected to high-velocity impact using the finite element model (FEM). The FEM was validated with experimental tests by comparing the numerical and experimental residual velocity, ballistic limit and contact time.

Researchers such as Jover *et al.*^[7], Ryan *et al.*^[21], García-Castillo *et al.*^[23] and Feli *et al.*^[24] also have done some meaningful work. However, all these previous research works focused mainly on the ballistic limit of composite sandwich panels with honeycomb, foam or balsa cores, while studies on composite sandwich panels with glass fiber-reinforced plastic (GFRP) cores and steel skins were relatively few.

The objective of this work is to develop an analytical model for the ballistic limit of the composite sandwich panels with a GFRP core subjected to high-velocity impact of a flat-nosed cylindrical projectile. The front and back skins of the sandwich panel are made from steel. The perforation process is divided into three stages based on which the energy absorption and ballistic limit of the composite GFRP sand-

wich panels are estimated with the upsetting effect of the projectile taken into consideration. The analytical model is validated by comparing the analytical solutions with the experimental results.

1 Analytic Model

1.1 Problem and Assumptions

The impact problem under consideration is described in Fig. 1. The composite sandwich panel consists of FRP composite laminate cores sandwiched between two thin steel plates. The projectile considered is a steel cylindrical projectile with a flat nose. According to the law of conservation of energy, the conservation of energy reads

$$\frac{1}{2}mv_i^2 = E_{\text{abs}} + \frac{1}{2}m_c v_r^2 \quad (1)$$

where m is the mass of the projectile, m_c is the mass of combination projectile, E_{abs} is the total energy absorption during the penetration, v_i and v_r are the initial and residual velocity of the projectile, respectively.

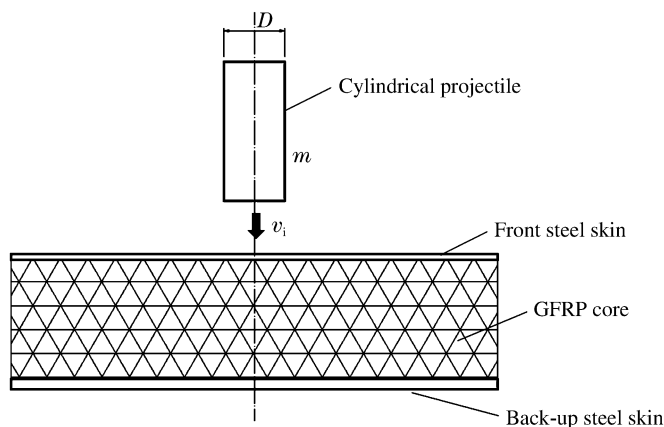


Fig. 1 Schematic diagram of composite sandwich panels under impact of flat-nose cylindrical projectile

The analytical model is based on the following assumptions: (1) The interfaces between front and back skins and GFRP composite laminate core are negligible and the energy absorptions of sheets and core are considered to be relatively independent; (2) The projectile is considered as a rigid body when penetrating the GFRP composite laminate; (3) The thickness of GFRP composite sandwich panel is uniform; (4) Only local deformation of steel skin is taken into consideration.

With different impact velocities and thicknesses, simply using the same calculation method on the front and back steel skins is unreasonable. With the above assumptions, the perforation process is divided into three stages (as shown in Fig. 2):

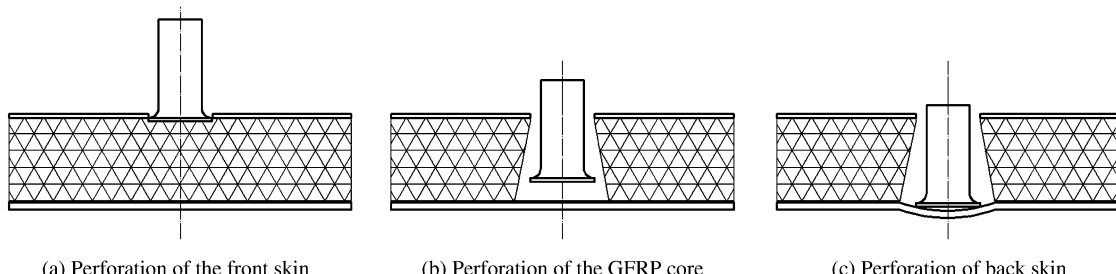


Fig. 2 Three stages of perforation

Stage 1: perforation of the front steel skin.

Stage 2: perforation of the GFRP composite laminate core.

Stage 3: perforation of the back steel skin.

The overall absorption energy consists of three parts

$$E_{\text{abs}} = E_{\text{fro}} + E_{\text{cor}} + E_{\text{bac}} \quad (2)$$

where E_{fro} , E_{cor} , E_{bac} stand for the energy absorption of stage 1, stage 2 and stage 3, respectively.

1.2 Perforation of Front Steel Skin

In the process of the projectile penetration, the overall deformation of the front steel skin is so small because of the support of the GFRP composite laminate that it can be neglected. Under the high-speed projectile impact, the projectile and the sheared part of the front skin form a closed region where most of the plastic work is converted into heat instead of getting lost instantly into the surrounding area. The temperature of the shear area increases rapidly, along with the effects of strain hardening, strain rate enhanced and thermal softening. The failure mode of the front steel skin is considered as localized adiabatic shear plugging.

When the cylindrical projectile starts to penetrate, the front skin is gradually extruded by the projectile. With the deepening of the penetration, the projectile velocity gradually decreases with the increase of the velocity of the plug block. Due to the compression, the axial compression deformation is produced by the projectile (as shown in Fig. 2). Assuming that the projectile and the plug block move together at a common speed, the diameter of the projectile after having the upsetting is d , and the common speed is v_c , then, according to the law of conservation of momentum, we have

$$mv_{i,1} = (m + m_f)v_c \quad (3)$$

Here $v_{i,1}$ is the initial velocity of the projectile in the first stage, m_f is the mass of the plug block which can be expressed as

$$m_f = \pi d^2 h_f \rho_f / 4 \quad (4)$$

where h_f and ρ_f are the thickness and density of the front skin, respectively.

Based on the stress wave theory, the relation of the diameters of the projectile before and after the upsetting can be expressed as^[25]

$$\begin{cases} c_1 = d^2 / D^2 \\ c_1 = k_1 + 1 + \sqrt{k_1^2 + 2k_1} \\ k_1 = 3\rho v_{i,1}^2 / (8\sigma_y) \end{cases} \quad (5)$$

where D is the initial diameter of the projectile, ρ is the density of the projectile, and σ_y is the dynamic yield strength of projectile.

Regardless of the energy loss of collision, according to the law of conservation of energy, the energy loss in the penetration process is equal to

$$E_{\text{fro}} = \frac{m + m_f}{2} (v_{i,1}^2 - v_{r,1}^2) = \pi d h_f \int_0^{P_m} \tau dP \quad (6)$$

where $v_{r,1}$ is the residual velocity of the projectile after the penetration of the front steel skin, and P_m is the maximum penetration depth when the adiabatic shear occurs. Based on the Bai-Johnson thermal-plastic constitutive relation^[25], τ can be written as

$$\tau = \tau_M \left(\frac{\gamma}{\gamma_i} \right) \exp \left\{ \frac{n}{n+1} \left[1 - \left(\frac{\gamma}{\gamma_i} \right)^{n+1} \right] \right\} \quad (7)$$

The Bai-Johnson thermal-plastic constitutive relation is shown in Fig. 3, where τ_M is the critical stress of the adiabatic instability of the front skin, γ_i is the corresponding shear strain of the critical stress,

and n is the strain hardening index.

The ultimate shear stress of the front steel skin can be written as^[26]

$$\tau_u = \sigma_u (0.41H/D + 0.42) \quad (8)$$

where τ_u is the ultimate shear stress, σ_u is the ultimate tensile stress, H is the thickness of the front steel skin, and $H = h_f$. Using $\tau_u = \tau_M$ as a first order approximation, after considering the upsetting effect, substituting Eq. (8) into Eq. (7) gives

$$\tau_u = \sigma_u \left(0.41 \frac{H}{D} + 0.42 \right) \left(\frac{\gamma}{\gamma_i} \right)^n \exp \left\{ \frac{n}{n+1} \left[1 - \left(\frac{\gamma}{\gamma_i} \right)^{n+1} \right] \right\} \quad (9)$$

The penetration depth can be expressed as^[25]

$$P = \frac{nd\gamma_a}{2(1+n)} \quad (10)$$

where γ_a is the shear strain of the contact area of the projectile and the front steel skin. Using $\gamma_a = \gamma_f$, the maximum penetration depth (P_m) at the time when the adiabatic shear plugging failure occurs can be written as

$$P_m = \frac{nd\gamma_f}{2(1+n)} \quad (11)$$

where γ_f is the maximum shear strain of the adiabatic shear band. The crack propagation speed of the front steel skin is faster than the penetrating speed as the flat-nosed projectile penetrates the front steel skin. The experimental results show that the maximum penetration depth (P_m) is less than the thickness of the front steel skin^[27]. Using $P_m \approx 0.8h_f$, Eq. (11) can be transformed as

$$\gamma_f = \frac{n+1}{n} \frac{2P_m}{d} = \frac{1.6(1+n)h_f}{nd} \quad (12)$$

Substituting Eq. (9), Eq. (11) and Eq. (12) into Eq. (6) gives

$$E_{fro} = \frac{\pi}{2} d^2 h_f \sigma_u \left[0.41 \frac{h_f}{d} + 0.42 \right] \int_0^{\frac{1.6h_f(1+n)}{nd}} \left(\frac{\gamma}{\gamma_i} \right)^n \exp \left\{ \frac{n}{n+1} \left[1 - \left(\frac{\gamma}{\gamma_i} \right)^{n+1} \right] \right\} d\gamma \quad (13)$$

Eq. (13) represents the penetration energy of the projectile in the first stage. The above derivation does not take the energy dissipation of the overall deformation of the front steel skin into account, because the overall deformation of the front skin is very small when the adiabatic shear failure occurs. According to the law of conservation of energy, the residual velocity of the projectile after the penetration of the front steel skin ($v_{r,1}$) can be obtained

$$v_{r,1} = \sqrt{\frac{mv_{i,1}^2 - 2E_{fro}}{m+m_f}} \quad (14)$$

1.3 Perforation of GFRP Composite Laminate

It is assumed that the mean pressure (σ_m) applied normally to the surface of the projectile provided by an GFRP laminate material to resist penetration and perforation by a projectile can be divided into two parts, one being the cohesive quasi-static resistive pressure (σ_s) due to the elastic-plastic deformation of the laminate and the other is the dynamic resistive pressure (σ_d) arising from the velocity effect^[9]. Thus we get the following equation

$$\sigma_m = \sigma_s + \sigma_d \quad (15)$$

Assuming that the cohesive quasi-static resistive pressure is equal to the quasi-static linear elastic limit (σ_e) in the through-thickness compression of the FRP laminate, i.e. $\sigma_s = \sigma_e$, and that the dynamic

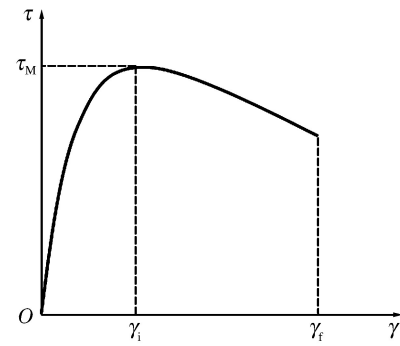


Fig. 3 Bai-Johnson thermal-plastic constitutive model

Fig. 3

Bai-Johnson thermal-plastic constitutive model

Fig. 3

Bai-Johnson thermal-plastic constitutive model

Fig. 3

Bai-Johnson thermal-plastic constitutive model

Fig. 3

Bai-Johnson thermal-plastic constitutive model

Fig. 3

Bai-Johnson thermal-plastic constitutive model

Fig. 3

Bai-Johnson thermal-plastic constitutive model

Fig. 3

Bai-Johnson thermal-plastic constitutive model

Fig. 3

Bai-Johnson thermal-plastic constitutive model

Fig. 3

Bai-Johnson thermal-plastic constitutive model

Fig. 3

Bai-Johnson thermal-plastic constitutive model

Fig. 3

Bai-Johnson thermal-plastic constitutive model

Fig. 3

Bai-Johnson thermal-plastic constitutive model

Fig. 3

Bai-Johnson thermal-plastic constitutive model

Fig. 3

Bai-Johnson thermal-plastic constitutive model

Fig. 3

Bai-Johnson thermal-plastic constitutive model

Fig. 3

Bai-Johnson thermal-plastic constitutive model

Fig. 3

Bai-Johnson thermal-plastic constitutive model

Fig. 3

Bai-Johnson thermal-plastic constitutive model

Fig. 3

Bai-Johnson thermal-plastic constitutive model

Fig. 3

Bai-Johnson thermal-plastic constitutive model

Fig. 3

Bai-Johnson thermal-plastic constitutive model

Fig. 3

Bai-Johnson thermal-plastic constitutive model

Fig. 3

Bai-Johnson thermal-plastic constitutive model

Fig. 3

Bai-Johnson thermal-plastic constitutive model

Fig. 3

Bai-Johnson thermal-plastic constitutive model

Fig. 3

Bai-Johnson thermal-plastic constitutive model

Fig. 3

Bai-Johnson thermal-plastic constitutive model

Fig. 3

Bai-Johnson thermal-plastic constitutive model

Fig. 3

Bai-Johnson thermal-plastic constitutive model

Fig. 3

Bai-Johnson thermal-plastic constitutive model

Fig. 3

Bai-Johnson thermal-plastic constitutive model

Fig. 3

Bai-Johnson thermal-plastic constitutive model

Fig. 3

Bai-Johnson thermal-plastic constitutive model

Fig. 3

Bai-Johnson thermal-plastic constitutive model

Fig. 3

Bai-Johnson thermal-plastic constitutive model

Fig. 3

Bai-Johnson thermal-plastic constitutive model

Fig. 3

Bai-Johnson thermal-plastic constitutive model

Fig. 3

Bai-Johnson thermal-plastic constitutive model

Fig. 3

Bai-Johnson thermal-plastic constitutive model

Fig. 3

Bai-Johnson thermal-plastic constitutive model

Fig. 3

Bai-Johnson thermal-plastic constitutive model

Fig. 3

Bai-Johnson thermal-plastic constitutive model

Fig. 3

Bai-Johnson thermal-plastic constitutive model

Fig. 3

Bai-Johnson thermal-plastic constitutive model

Fig. 3

Bai-Johnson thermal-plastic constitutive model

Fig. 3

Bai-Johnson thermal-plastic constitutive model

Fig. 3

Bai-Johnson thermal-plastic constitutive model

Fig. 3

Bai-Johnson thermal-plastic constitutive model

Fig. 3

Bai-Johnson thermal-plastic constitutive model

Fig. 3

Bai-Johnson thermal-plastic constitutive model

Fig. 3

Bai-Johnson thermal-plastic constitutive model

Fig. 3

Bai-Johnson thermal-plastic constitutive model

Fig. 3

Bai-Johnson thermal-plastic constitutive model

Fig. 3

Bai-Johnson thermal-plastic constitutive model

Fig. 3

Bai-Johnson thermal-plastic constitutive model

Fig. 3

Bai-Johnson thermal-plastic constitutive model

Fig. 3

Bai-Johnson thermal-plastic constitutive model

Fig. 3

Bai-Johnson thermal-plastic constitutive model

Fig. 3

Bai-Johnson thermal-plastic constitutive model

Fig. 3

Bai-Johnson thermal-plastic constitutive model

Fig. 3

Bai-Johnson thermal-plastic constitutive model

Fig. 3

Bai-Johnson thermal-plastic constitutive model

Fig. 3

Bai-Johnson thermal-plastic constitutive model

Fig. 3

Bai-Johnson thermal-plastic constitutive model

Fig. 3

Bai-Johnson thermal-plastic constitutive model

Fig. 3

Bai-Johnson thermal-plastic constitutive model

Fig. 3

Bai-Johnson thermal-plastic constitutive model

Fig. 3

Bai-Johnson thermal-plastic constitutive model

Fig. 3

Bai-Johnson thermal-plastic constitutive model

Fig. 3

Bai-Johnson thermal-plastic constitutive model

Fig. 3

Bai-Johnson thermal-plastic constitutive model

Fig. 3

Bai-Johnson thermal-plastic constitutive model

Fig. 3

Bai-Johnson thermal-plastic constitutive model

Fig. 3

Bai-Johnson thermal-plastic constitutive model

Fig. 3

Bai-Johnson thermal-plastic constitutive model

Fig. 3

Bai-Johnson thermal-plastic constitutive model

Fig. 3

Bai-Johnson thermal-plastic constitutive model

Fig. 3

Bai-Johnson thermal-plastic constitutive model

Fig. 3

Bai-Johnson thermal-plastic constitutive model

Fig. 3

Bai-Johnson thermal-plastic constitutive model

Fig. 3

Bai-Johnson thermal-plastic constitutive model

Fig. 3

Bai-Johnson thermal-plastic constitutive model

Fig. 3

Bai-Johnson thermal-plastic constitutive model

Fig. 3

Bai-Johnson thermal-plastic constitutive model

Fig. 3

Bai-Johnson thermal-plastic constitutive model

Fig. 3

Bai-Johnson thermal-plastic constitutive model

Fig. 3

Bai-Johnson thermal-plastic constitutive model

Fig. 3

Bai-Johnson thermal-plastic constitutive model

Fig. 3

Bai-Johnson thermal-plastic constitutive model

Fig. 3

Bai-Johnson thermal-plastic constitutive model

Fig. 3

Bai-Johnson thermal-plastic constitutive model

Fig. 3

Bai-Johnson thermal-plastic constitutive model

Fig. 3

Bai-Johnson thermal-plastic constitutive model

Fig. 3

Bai-Johnson thermal-plastic constitutive model

Fig. 3

Bai-Johnson thermal-plastic constitutive model

Fig. 3

Bai-Johnson thermal-plastic constitutive model

Fig. 3

Bai-Johnson thermal-plastic constitutive model

Fig. 3

Bai-Johnson thermal-plastic constitutive model

Fig. 3

Bai-Johnson thermal-plastic constitutive model

Fig. 3

Bai-Johnson thermal-plastic constitutive model

Fig. 3

Bai-Johnson thermal-plastic constitutive model

Fig. 3

Bai-Johnson thermal-plastic constitutive model

Fig. 3

Bai-Johnson thermal-plastic constitutive model

Fig. 3

Bai-Johnson thermal-plastic constitutive model

Fig. 3

Bai-Johnson thermal-plastic constitutive model

Fig. 3

Bai-Johnson thermal-plastic constitutive model

Fig. 3

Bai-Johnson thermal-plastic constitutive model

Fig. 3

Bai-Johnson thermal-plastic constitutive model

resistive pressure is taken to be $\sigma_d = \beta(\rho_e/\sigma_e)^{1/2} v_{i,2} \sigma_e$, then Eq. (14) can be rewritten as

$$\sigma_m = \left(1 + \beta v_{i,2} \sqrt{\frac{\rho_e}{\sigma_e}}\right) \sigma_e \quad (16)$$

where ρ_e is the density of the GFRP composite laminate, $v_{i,2}$ is the initial impact velocity of the projectile in the second stage, here $v_{i,2} = v_{r,1}$, and β is a constant determined empirically.

From the energy conservation, the energy loss of the GFRP cores can be written as

$$E_{cor} = \int_0^{h_c} \sigma_m A dh \quad (17)$$

where A is the instant cross-sectional area of the projectile and is equal to $\pi d^2/4$. Substituting Eq. (16) into Eq. (17) gives

$$E_{cor} = \frac{1}{4} \pi d^2 \left(\sigma_e + 2 \sqrt{\frac{\rho_e}{\sigma_e}} v_{r,1} \sigma_e \right) h_c \quad (18)$$

Then the residual velocity of the projectile after the penetration of the GFRP laminate ($v_{r,2}$) can be obtained

$$v_{r,2} = \sqrt{\frac{mv_{i,1}^2 - 2(E_{fro} + E_{cor})}{m + m_f}} \quad (19)$$

1.4 Perforation of Back Steel Skin

The penetration process is shown in Fig. 4. A three-stage model consisting of the simple compression stage, the compression-shear stage and the adiabatic shear stage is used to describe the penetration process of the back steel skin. Assuming that the projectile upsetting deformation only occurs in the simple compression stage and the upsetting length is equal to the penetration depth (h_1), then, based on Eq. (5), the relation of diameters of the projectile before and after upsetting can be expressed as

$$\begin{cases} c_2 = \frac{d_2^2}{d^2} \\ c_2 = k_2 + 1 + \sqrt{k_2^2 + 2k_2} \\ k_2 = \frac{3\rho v_{i,3}^2}{8\sigma_y} \end{cases} \quad (20)$$

where d_2 is the diameter of the projectile after the upsetting deformation. Then the energy loss of the simple compression stage can be expressed as

$$W_1 = \frac{1}{2}(m + m_f)(v_{i,3}^2 - v_1^2) = \frac{1}{4}\pi d_2^2 \sigma_y h_1 \quad (21)$$

where v_1 is the residual velocity of the projectile after the simple compression stage and can be written as follows

$$v_1 = \sqrt{v_{i,3}^2 - \frac{\pi d_2^2 \sigma_y h_1}{2(m + m_f)}} \quad (22)$$

After the simple compression stage, the projectile continues to compress the back steel skin. The relative movement of the plug block and the back steel skin leads to the existence of shear stress. Under the action of the compression force, the projectile and the shear block will reach the same speed. Assuming that the diameter of the plug block is equal to d_2 , the projectile and plug block will reach the same speed under the effect of the compressive stress. According to the law of conservation of momentum, one obtains

$$v_2 = \frac{(m + m_f)v_1}{m + m_f + m_b} \quad (23)$$

Here m_b is the mass of the plug block and can be expressed as

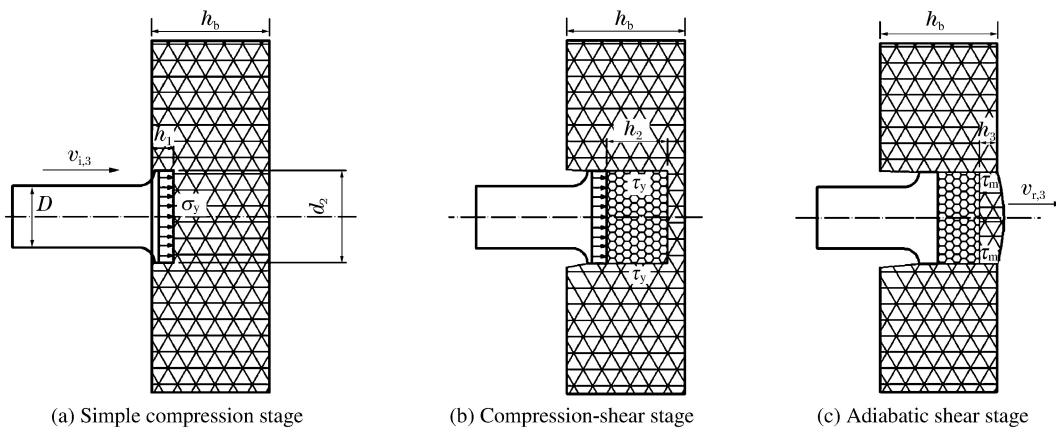


Fig. 4 Penetration of the back skin

$$m_b = \frac{1}{4} \rho_b \pi d_2^2 (h_b - h_1) \quad (24)$$

where ρ_b and h_b are the density and thickness of the back skin, respectively. Then, according to the law of conservation of energy, the energy loss of the compression-shear stage can be written as

$$W_2 = \frac{1}{2} (m + m_f) v_1^2 - \frac{1}{2} (m + m_f + m_b) v_2^2 \quad (25)$$

With the deepening of the penetration, the temperature as well as the shear strain of the shear zone rises gradually. The material adiabatic instability occurs when the shear strain reaches its critical value (γ_i). Assuming that the penetration depth of the projectile in adiabatic shear stage is h_3 , according to Eq. (13), the energy loss of the adiabatic shear stage can be written as

$$W_3 = \frac{\pi}{2} d_2^2 h_3 \sigma_u \left[0.41 \frac{h_3}{d_2} + 0.42 \right] \int_0^{h_3} \left(\frac{\gamma}{\gamma_i} \right)^n \exp \left\{ \frac{n}{n+1} \left[1 - \left(\frac{\gamma}{\gamma_i} \right)^{n+1} \right] \right\} d\gamma \quad (26)$$

Then the total energy loss of the perforation of the back steel skin is

$$E_{bac} = W_1 + W_2 + W_3 \quad (27)$$

When the initial velocity (v_i) equals to the ballistic limit (v_{bl}), the residual velocity (v_r) of the projectile after the adiabatic shear stage is considered to be zero. Combining Eq. (1) and Eq. (2), one obtains

$$mv_{bl}^2 - 2(E_{cor} + E_{fro} + E_{bac}) = 0 \quad (28)$$

Solving Eq. (28), one can get the ballistic limit of the composite sandwich panel with GFRP core.

2 Experimental Verification of the Analytical Model

To study the ballistic limit of the composite sandwich plate, the experimental study on the ballistic impact and penetration of the composite GFRP sandwich panel is carried out. The sandwich panels are quadratic with the size of 500 mm × 500 mm. Panels have steel skins separated by GFRP composite laminate core. The thicknesses of the front skin and back skin are 6.2 mm and 10.6 mm, respectively. The mechanical and geometrical properties of the steel skins are shown in Table 1. The density and quasi-static linear elastic limit of GFRP composite laminate core are 1650 kg/m³ and 225 MPa, respectively. The thickness of the GFRP composite laminate varies from 40 mm to 75 mm.

Table 1 Mechanical and geometrical properties of steel skins

h_f/mm	h_b/mm	$\rho_f/(\text{kg} \cdot \text{m}^{-3})$	σ_u/MPa	n	γ_i
6.2	10.6	7850	779	0.586	1.4

The projectile is cylindrical with the mass ranging from 30 g to 50 g and the diameter $D=12.8$ mm. The density and the dynamic yield strength of the projectile are 7750 kg/m^3 and 1280 MPa, respectively. The incident angle is 90° .

The experimental setup is shown schematically in Fig. 5. In order to provide the clamped boundary conditions, the steel skins and the GFRP core are bolt fastened together through 4 $\varnothing 10$ mm bolts which are located in the 4 corners of the plate.

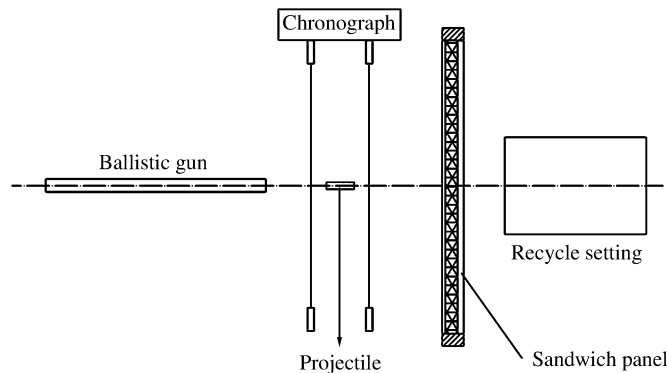


Fig. 5 Experimental setup of the ballistic impact on sandwich panels

The projectile is fired through the ballistic gun, and the initial velocity (v_i) is measured by the time difference of the projectile passing through the two light-emitter/sensor pairs. A recycle setting is provided to stop the projectile from hitting the back wall when the sandwich panel is perforated. Incident and residual velocities of the projectile are measured with high precision and the ballistic limit of the sandwich panel is estimated using statistical method. Considering the high-speed projectile impact, the initial striking velocity varies from 900 m/s to 1700 m/s.

2.1 Experimental Study on Damage Mechanisms

Consider the perforation of the sandwich composite plate with a 60 mm thick GFRP core as a typical case. The plastic deformation of the front skin is shown in Fig. 6. A visual examination reveals that the front skin only shows up localized plastic deformation and the diameter of the hole is a bit larger than the diameter of the projectile. It is illustrated that the upsetting phenomenon occurs on the projectile during perforation of the front skin. Fig. 6(a) shows the plug block is produced and Fig. 6(b) presents an obvious adiabatic shear band which proves the failure mode of the front skin to be local adiabatic shear-plugging failure.



Fig. 6 Plastic deformation of the front skin

The 60 mm thick GFRP core consists of 3 layers of 20 mm thick composite laminates. The plastic deformation of each layer is shown in Fig. 7. It is illustrated that the overall deformation of the first

layer is very small, which gives a good support to the front skin. The failure mode of the front side fiber under high-speed projectile impact is compression shear failure while the failure mode of the back side fiber is tensile failure. With the deepening of the penetration, the overall deformation of the GFRP composite laminate gradually increases due to the compression and shearing between the projectile and the composite laminate. However, the existence of the back skin imposes a restriction on this trend. Besides, a large amount of heat produced by the hypervelocity penetration leads to the firing of the fibers.

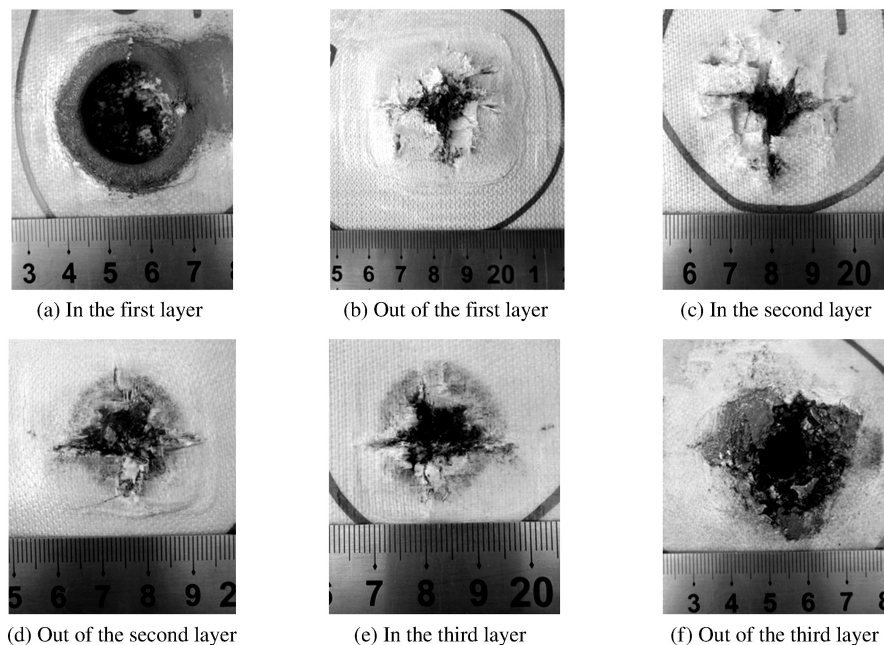


Fig. 7 Plastic deformation of GERP core

The plastic deformation of the back skin is shown in Fig. 8. As is shown, except for the localized plastic shear deformation, a small overall deformation occurred to the back steel skin as a result of the compression between the projectile and the back skin. After the penetration of the face skin and the GFRP core, the speed of the projectile is relatively low when the projectile penetrates the back skin. The shape of the projectile after the perforation of the back skin is shown in Fig. 9. The shapes of the projectile and bullet hole show that the main failure mode of the back skin is the simple shear plugging failure, which is similar to the penetration characteristics of the mid-thick steel plate. However, a small adiabatic shear band exists in the edge of the bullet hole (shown in Fig. 8(b)).

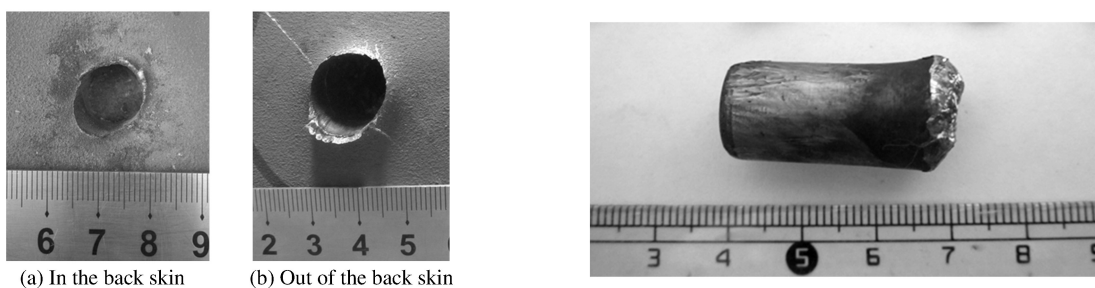


Fig. 8 Plastic deformation of the back skin

Fig. 9 Shape of projectile after perforation of back skin

The experiment results show that the failure mode of the composite sandwich plate is consistent with the theoretical model established in this paper. The front and back steel skins will produce a large

deformation when subjected to the projectile impact due to their good ductility. The tensile strength of the fiber reinforced composite material is higher than that of the steel whereas, however, little plastic deformation occurs before reaching its tensile strength. This kind of characteristic effectively restrains the deformation of the steel skins. The existence of the back skin can provide a last barrier to resist against the projectile as much as possible. Therefore, the steel skins are typically responsible for bearing the in-plane load, whereas the GFRP core serves to transfer the shear between the front and back skins and restrain the overall deformation of the composite sandwich plate.

2.2 Comparison of Results and Discussion

One may find a summary of the experimental data for the sandwich composite panels with a 60 mm thick GFRP core in Fig. 10 where the ballistic limit is marked up using a red line. The conditions between exact perforation and near perforation are considered as the critical state of which the corresponding incidence velocity is considered as the critical velocity. Obviously, there are 15 cases conducted, the ballistic limit is obtained using the statistical method from the critical values. The standard deviation of the ballistic limit is 18.91 m/s.

As it is shown in Table 2, five ballistic tests with 3 different core thicknesses and 3 different projectile masses are conducted. Due to the constraints, we failed to gain the data for two conditions of the five. The test values of the two failed conditions given in Table 2 are the maximum speed of the projectile, one projectile of which is almost through the panel while the other is not. The theoretical values of the ballistic limits are calculated following Eq. (28). Comparison of the test and theoretical results is listed in Table 2.

Notice that the errors of the ballistic limit between the test results and the theoretical results is less than 11%, which is within the limit of engineering requirements. It should be mentioned that the experimental evaluation of the ballistic limit is uncertain to some degree for the limited amount of data and measurement error. The calculated value of the ballistic limit of the sandwich plate with a 40 mm thick core is relatively large. This is because the support effective of GFRP cores is relatively weaker than the other conditions so that the bearing capacity of the front skin has been overestimated.

In order to further explore the ballistic impact characteristics of the composite GFRP sandwich panels, some numerical results are obtained based on the theoretical formula in this paper. The energy absorption ratio of each stage under the condition of the ballistic limit velocity is shown in Table 3. It is shown that more than 90% energy is absorbed by the GFRP composite laminate and less than 10% by the steel skins. Only very little plastic deformation occurred to the steel skins of both sides because of its low energy absorption. It is also proved that the energy absorption of the fiber compression and fracture is much larger than the shear energy dissipation of the steel skins.

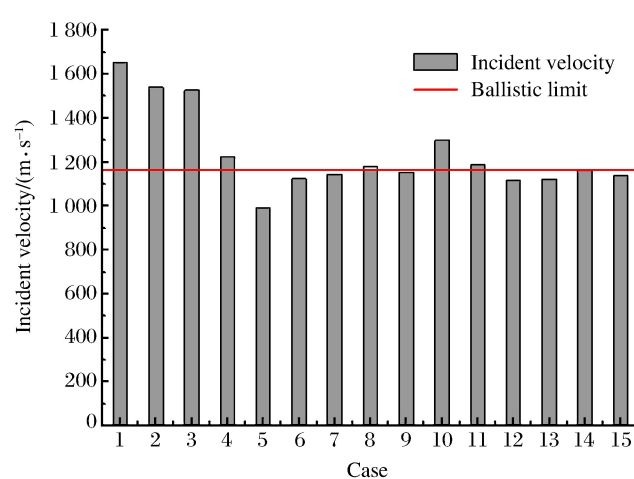


Fig. 10 Experimental data of sandwich composite panels with a 60 mm thick GFRP core under impact of flat-nosed cylindrical projectile

Table 2 Comparison of ballistic limit computed by theoretical model with experimental results

Mass/g	Core thickness/mm	Exp. value/(m · s ⁻¹)	Calc. value/(m · s ⁻¹)	Error/%
40	40	753.8	831.9	10.7
30	60	1 422.9	1 402.9	—
40	60	1 162.7	1 132.4	2.6
50	60	974.1	958.1	1.6
50	75	879.0	1 144.7	—

Fig. 11 shows that the ballistic limit of the composite GFRP sandwich panel presents a linear increase trend with the increase of the core thickness. On the other hand, a nonlinear decline of the ballistic limit of the composite GFRP sandwich panel with the increase of the mass of projectile is shown in Fig. 12. It is evident from these two figures that the theoretically predicted ballistic limits are in good agreement with the experimental data. As a matter of fact, the mass of both the projectile and the core thickness exerts a significant influence on the ballistic limit, which provides a reference for the penetration resistance design standards.

Table 3 Energy absorption ratio of composite GFRP sandwich panels under impact of flat-nosed cylindrical projectile with ballistic limit velocity

Mass/g	Core thickness/mm	(E _{fro} /E _{abs})/%	(E _{cor} /E _{abs})/%	(E _{bac} /E _{abs})/%
40	40	2.9	90.7	6.4
30	60	1.6	95.0	3.4
40	60	1.4	95.7	2.9
50	60	1.8	94.4	3.8
50	75	1.2	96.1	2.7

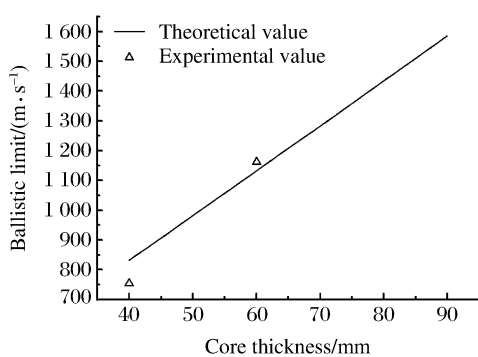


Fig. 11 Ballistic limit changing with the GFRP core thickness under impact of a 40 g flat-nosed cylindrical projectile

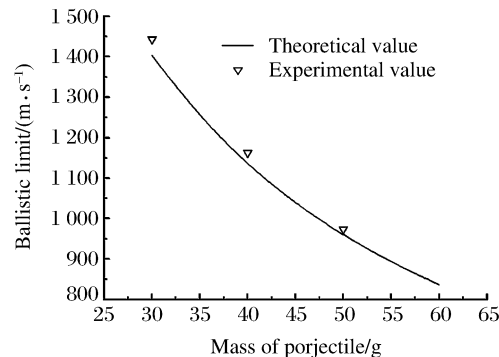


Fig. 12 Ballistic limit of composite GFRP sandwich panels with a 60 mm thick core changing with the mass of projectile

3 Conclusions

In this study, a theoretical approach is developed for the penetration and perforation of the composite GFRP sandwich panels struck transversely by the cylindrical projectiles with a flat nose over a wide range of impact velocity, mass of the projectile and thickness of the core. The approach is based upon a three-stage model with the assumption that the deformations of the steel skins are localized and the projectile is considered as a rigid body in the perforation of the GFRP composite laminate. The energy absorption of the sandwich panels is divided into three parts, *i.e.* the energy absorption of the front skin, that of the GFRP core, and that of the back skin. The adiabatic shear model and simple

shear model are used to predict the energy absorption of the front skin and the back skin, respectively, with the upsetting effect of the projectile taken into consideration. Analytical solutions have been derived for the penetration depth and the ballistic limit in the case of perforation.

It is demonstrated that the theoretical predictions are in good agreement with the experimental observations for the composite GFRP sandwich panels struck normally by the cylindrical projectiles with a flat nose in terms of the penetration depth and the ballistic limit. Numerical calculation is carried out based on the theoretical formula proposed in this paper, which indicates the significant influences of the projectile mass and the core thickness on the ballistic limit.

References:

- [1] JOHNSON W S, MASTERS J E, WILSON D W, et al. Comparison of the low and high velocity impact response of kevlar fiber-reinforced epoxy composites [J]. Journal of Composites Technology & Research, 1999, 21(4): 224-229.
- [2] VAIDYA U K, ULVEN C, PILLAY S, et al. Impact damage of partially foam-filled co-injected honeycomb core sandwich composites [J]. Journal of Composite Materials, 2003, 37(7): 611-626.
- [3] KEPLER J. Impact penetration of sandwich panels at different velocities—an experimental parameter study: part I—parameters and results [J]. Journal of Sandwich Structures & Materials, 2004, 6(4): 357-374.
- [4] 曹海要, 战再吉. 铜/金刚石复合材料电磁轨道烧蚀特性的实验研究 [J]. 高压物理学报, 2016, 30(4): 317-322.
CAO H Y, ZHAN Z J. Experimental study of Cu/diamond composite electromagnetic rail ablation characteristics [J]. Chinese Journal of High Pressure Physics, 2016, 30(4): 317-322.
- [5] 王志刚, 徐亮, 李绪海, 等. 碳化硅-金刚石超硬复合材料的弹性性质 [J]. 高压物理学报, 2015, 29(4): 263-267.
WANG Z G, XU L, LI X H, et al. Elastic property of SiC-diamond composite under hydrostatic pressure [J]. Chinese Journal of High Pressure Physics, 2015, 29(4): 263-267.
- [6] LI G, JONES N. Development of rubberized syntactic foam [J]. Composites Part A: Applied Science and Manufacturing, 2007, 38(6): 1483-1492.
- [7] JOVER N, SHAFIQ B, VAIDYA U. Ballistic impact analysis of balsa core sandwich composites [J]. Composites Part B: Engineering, 2014, 67: 160-169.
- [8] NIA A A, RAZAVI S B, MAJZOobi G H. Ballistic limit determination of aluminum honeycombs—experimental study [J]. Materials Science and Engineering A, 2008, 488(1/2): 273-280.
- [9] WEN H M. Predicting the penetration and perforation of FRP laminates struck normally by projectiles with different nose shapes [J]. Composite Structures, 2000, 49(3): 321-329.
- [10] WEN H M. Penetration and perforation of thick FRP laminates [J]. Composites Science & Technology, 2001, 61(8): 1163-1172.
- [11] GU B. Analytical modeling for the ballistic perforation of planar plain-woven fabric target by projectile [J]. Composites Part B: Engineering, 2003, 34(4): 361-371.
- [12] NAIK N K, DOSHI A V. Ballistic impact behaviour of thick composites: parametric studies [J]. Composite Structures, 2008, 82(3): 447-464.
- [13] NAIK N K, SHRIRAO P, REDDY B C K. Ballistic impact behaviour of woven fabric composites: formulation [J]. International Journal of Impact Engineering, 2006, 32(9): 1521-1552.
- [14] GAMA B A, GILLESPIE J W Jr. Punch shear based penetration model of ballistic impact of thick-section composites [J]. Composite Structures, 2008, 86(4): 356-369.
- [15] CHAN S, FAWAZ Z, BEHDINAN K, et al. Ballistic limit prediction using a numerical model with progressive damage capability [J]. Composite Structures, 2007, 77(4): 466-474.
- [16] FELI S, YAS M H, ASGARI M R. An analytical model for perforation of ceramic/multi-layered planar woven fabric targets by blunt projectiles [J]. Composite Structures, 2011, 93(2): 548-556.
- [17] SILVA M A G, CISMASIU C, CHIOREAN C G. Numerical simulation of ballistic impact on composite laminates

- [J]. International Journal of Impact Engineering, 2005, 31(3): 289-306.
- [18] GOLDSMITH W, WANG G T, LI K, et al. Perforation of cellular sandwich plates [J]. International Journal of Impact Engineering, 1997, 19(5/6): 361-379.
- [19] SKVORTSOV V, KEPLER J, BOZHEVOLNAYA E. Energy partition for ballistic penetration of sandwich panels [J]. International Journal of Impact Engineering, 2003, 28(7): 697-716.
- [20] ZHOU D W, STRONGE W J. Ballistic limit for oblique impact of thin sandwich panels and spaced plates [J]. International Journal of Impact Engineering, 2008, 35(11): 1339-1354.
- [21] RYAN S, SCHAEFER F, DESTEFANIS R, et al. A ballistic limit equation for hypervelocity impacts on composite honeycomb sandwich panel satellite structures [J]. Advances in Space Research, 2008, 41(7): 1152-1166.
- [22] BUITRAGO B L, SANTIUSTE C, SANCHEZ-SAEZ S, et al. Modelling of composite sandwich structures with honeycomb core subjected to high-velocity impact [J]. Composite Structures, 2010, 92(9): 2090-2096.
- [23] GARCIA-CASTILLO S K, BUITRAGO B L, BARBERO E. Behavior of sandwich structures and spaced plates subjected to high-velocity impacts [J]. Polymer Composites, 2011, 32(2): 290-296.
- [24] FELI S, POUR M H N. An analytical model for composite sandwich panels with honeycomb core subjected to high-velocity impact [J]. Composites Part B, 2012, 43(5): 2439-2447.
- [25] BAI Y L, JOHNSON W. Plugging: physical understanding and energy absorption [J]. Materials Science & Technology, 2013, 9(1): 182-190.
- [26] LANGSETH M, LARSEN P K. The behaviour of square steel plates subjected to a circular blunt ended load [J]. International Journal of Impact Engineering, 1992, 12(4): 617-638.
- [27] BORVIK T, LANGSETH M, HOPPERSTAD O S, et al. Ballistic penetration of steel plates [J]. International Journal of Impact Engineering, 1999, 22(9/10): 855-886.

GFRP复合三明治板在高速弹体冲击下的 弹道极限预测

李思宇¹, 李晓彬¹, 赵鹏铎², 高松林¹

(1. 武汉理工大学交通学院,船舶、海洋与结构工程系,湖北 武汉 430063;
2. 海军装备研究院,北京 100073)

摘要:研究了玻璃纤维复合三明治板在圆柱形平头弹体打击下的预测弹道极限的理论预测方法。建立了玻璃纤维复合三明治板的三阶段侵彻模型,包括侵彻面板阶段、侵彻复合材料夹芯层阶段和侵彻内板阶段。基于高速弹体侵彻下靶板的局部变形假设建立了理论关系,将弹体侵彻复合材料夹心层时视为刚体处理,面板和背板的侵彻阶段考虑了弹体的墩粗效应和靶板的绝热剪切效应。基于能量平衡原理,推导了复合材料三明治板的弹道极限,并将理论计算结果与实验结果进行对比和分析,研究了不同侵彻速度、弹体质量和夹心层厚度对弹道极限的影响。结果表明,理论计算结果与实验结果具有较好的一致性。

关键词:弹道冲击;三明治结构;玻璃纤维增强;弹道极限

中图分类号: O385; TB33

文献标志码:A